Analyst

PAPER

View Article Online
View Journal

Cite this: DOI: 10.1039/c5an02134k

Nanopillar films with polyoxometalate-doped polyaniline for electrochemical detection of hydrogen peroxide†

MinHo Yang,[a] Dong Seok Kim,[b] Jo Hee Yoon,[b] Seok Bok Hong,[b] Soon Woo Jeong,[a] Dong Eun Yoo,[c] Tae Jae Lee,[a] Seok Jae Lee,*[a] Kyoung G. Lee*[a] and Bong Gill Choi*[b]

Received 16th October 2015,
Accepted 26th December 2015

DOI: 10.1039/c5an02134k

www.rsc.org/analyst

Design and fabrication of electrodes is key in the development of electrochemical sensors with superior electrochemical performances. Herein, an enzymeless electrochemical sensor is developed for detection of hydrogen peroxide based on the use of highly ordered polyoxometalate (POM)-doped polyaniline (PANI) nanopillar films. The electrodeposition technique enables the entrapment of POMs into PANI during electropolymerization to produce thin coatings of POM-PANI. Electrochemical investigations of the POM-PANI/nanopillar electrode showed well-defined multiple pairs of redox peaks and rapid electron transfer. The nanopillar structure facilitated the diffusion of the electrolyte and thus, enhanced the redox reaction. In particular, the POM-PANI/nanopillar electrode was incorporated into a flow injection biosensor and it demonstrates its electrocatalytic activity to detect hydrogen peroxide with high sensitivity, rapid response time, and low detection limit.

1. Introduction

Polyoxometalates (POMs), as anionic molecular metal–oxygen clusters, have attracted considerable attention as catalysts in the medicine and materials science fields due to their structural and compositional diversities and unique electronic, optical, and electrochemical properties.[1–5] In particular, POMs are capable of delivering reversible multielectron transfer reactions which makes them promising candidates for electrocatalytic reduction and oxidation reactions and for detecting biomarkers, such as hydrogen peroxide (H_2O_2), ascorbic acid, dopamine, and iodate in human blood.[6–9] However, the generally high solubility of POMs in aqueous solution hampers their applications in electrochemical devices. To overcome problems associated with solubility, several strategies have been recently developed to anchor POMs on electrode surfaces of conductive substrates using various deposition techniques, including layer-by-layer deposition, self assembly monolayers, Langmuir–Blodgett, sol–gel films, carbon-based hybridization, electrodeposition, and entrapment into conducting polymers.[4,6,10–13] Among them, incorporation into conducting polymers during electropolymerization is probably the most promising method because it is straightforward and provides efficient electrical communication between POMs and conducting polymers and stable *in situ* immobilization of the POMs.

The detection of H_2O_2 is important in the food, pharmaceutical, and environmental fields because it is a by-product of many oxidative biological reactions, including those of glucose oxidase, cholesterol oxidase, uricase, alcohol oxidase, galactose oxidase, sarcosine oxides, and L-amino-acid oxidase.[14–17] Most electrochemical sensors depend significantly on biological enzymes and soluble redox mediators, but enzyme based sensors often suffer from insufficient stability, poor tolerance under experimental conditions, poor reliability, and high cost. Recently, enzymeless electrochemical sensors based on noble metals or metal oxides have been proposed as alternatives for enzyme-based electrochemical sensors because of their enhanced better stabilities and reliabilities, and lower cost.[14–17]

Here, we report a robust enzymeless electrochemical sensor based on POM-doped polyaniline (POM-PANI) nanopillar film electrodes for the detection of H_2O_2. The highly ordered one dimensional (1D) structure of POM-PANI enabled efficient electron and ion transfer during electrochemical reactions. To evaluate the electrocatalytic performance of POM-PANI/nanopillar electrodes, we incorporated one into a flow injection biosensor device, leading to high sensitivity, rapid response time, and low detection limit.

[a]Department of Nano Bio Research, National NanoFab Center (NNFC), Daejeon 34141, Republic of Korea
[b]Department of Chemical Engineering, Kangwon National University, Samcheok 25913, Republic of Korea. E-mail: bgchoi@kangwan.ac.kr
[c]Device Process Technology Team, National NanoFab Center (NNFC), Daejeon 34141, Republic of Korea

†Electronic supplementary information (ESI) available. See DOI: 10.1039/c5an02134k

2. Experimental section

2.1 Preparation of POM-PANI/nanopillar electrodes

As previously described, nanopillar structured polymer films containing polyurethane acrylate and NOA63 were fabricated using a combined photo/soft-lithography process.[18] Prior to the deposition of POM and PANI, the nanopillar structured polymer films were coated with a thin layer of gold/titanium by vacuum sputtering. The as-synthesized films served as supporting electrodes for further electrodeposition of POMs and PANI. Briefly, POM-doped PANI films were synthesized using a co-electrodeposition process at a constant potential of 0.65 V for 400 s in a three electrode system. The electrolyte used was 0.5 M H_2SO_4 containing 0.25 M PANI and 20 mM POM. During the *in situ* electropolymerization of PANI, POMs were incorporated into the PANI matrix. After electrodeposition, POM-PANI/nanopillar films were washed several times with ethanol and deionized water and then dried under vacuum. As a reference sample, POM-PANI was deposited on the flat structured and gold/titanium-coated polymeric films by the same procedure for POM-PANI/nanopillar films.

2.2 Fabrication of enzymeless flow injection biosensors

Flow injection biosensors were fabricated by integrating a fluidic channel substrate with POM-PANI/nanopillar electrodes. The microfluidic devices were based on plastic substrates. The device was equipped with an inlet and an outlet hole, an Ag/AgCl reference electrode, and a Pt counter electrode. In addition, the microfluidic device included a syringe pump (KD Scientific, KDS 100) and a sample injector (Rhoedyne, model 7725i) with a 20 μL sample loop.

2.3 Characterization

Scanning electron microscopy (SEM) images were obtained using a field emission SEM (S-4800, Hitachi). Fourier transform infrared spectroscopy (FTIR) spectra were collected using a Bruker IFS 66v/S spectrometer coupled with a HYPERION 3000 IR microscope. All electrochemical measurements were performed on a CHI 760E electrochemical workstation (CH Instruments) using a conventional three-electrode system. Flow injection mode in biosensor was performed using a chronoamperometric technique. All flow injection measurements were carried out at a flow rate of 1 mL min^{-1}. Potentials were collected at room temperature, and data were obtained at an accuracy of ±1%. The sensitivity was calculated from the slope of the linear calibration curves at various concentrations of H_2O_2.

3. Results and discussion

Fig. 1 shows a schematic illustration for preparation of a POM-PANI/nanopillar film and a flow injection biosensor device. The POM-PANI/nanopillar films were fabricated by co-electrodeposition of POM and PANI onto previously prepared gold-coated polymeric substrates which was previously prepared by our group.[18] The employment of photo- and soft-lithography allowed us to fabricate large area nanopillar arrays with controllable sizes and arrangements. In addition, these nanopillar arrays could be transfered into various substrates, for example flexible plastics, metals, and textiles. In this study, we investigated the effects of nanopillar arrays on the electrochemical reactions of POM-PANI. Nanopillar structured polymer films produced by photo/soft-lithography were coated with a thin layer of gold nanoparticles. The POM and PANI were electrodeposited simultaneously onto this gold-coated polymeric nanopillar films. During the *in situ* electropolymerization of aniline, POMs were entrapped in the PANI matrix. In order to detect H_2O_2, we incorporated POM-PANI/nanopillar films as an electrode into the flow injection biosensor.

Fig. 2a shows POM-PANI/nanopillar films with dark green colar and they can be flexible. Compared to the bare nanopillar structure, deposition of POM-PANI created more rough surfaces with cone shape structures (Fig. 2c and d). The highly ordered nanopillar structure of POM-PANI had a diameter of

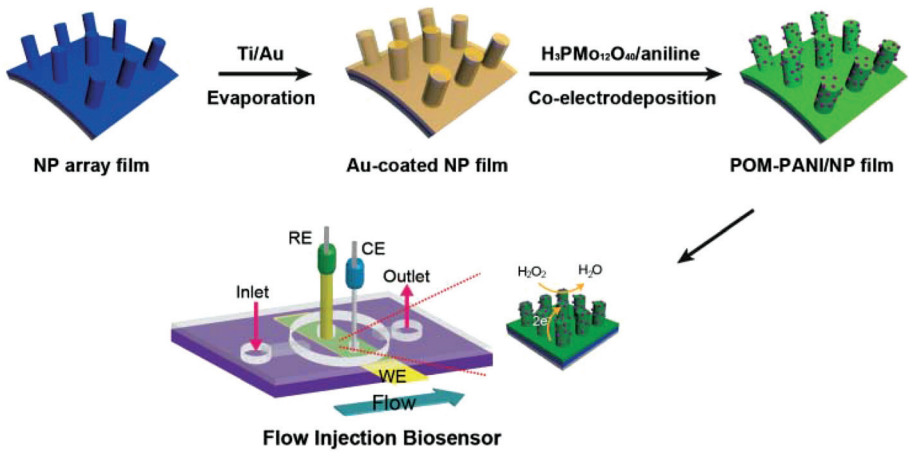

Fig. 1 Schematic illustration of the fabrication process for a POM-PANI/nanopillar film and flow injection biosensor device.

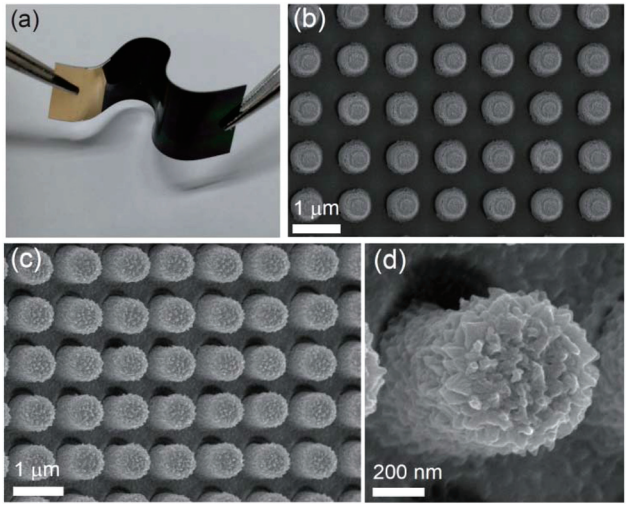

Fig. 2 (a) Photographic image of a POM-PANI/nanopillar film. (b) SEM image of a bare nanopillar film. (c) and (d) SEM images of a POM-PANI/nanopillar film at different magnifications.

~500 nm and inter-nanopillar distance of ~500 nm. The electrodeposition of POM and PANI enabled us to produce reproducibly thin coating layer on the nanopillar structures.

The FTIR spectra of POM-PANI/nanopillar films in Fig. 3 revealed unique bands corresponding to PANI and the phosphomolybdate anion, which indicated that the nanopillar films had been successfully coated with POM-PANI. The characteristic bands at 1572 and 1487 cm^{-1} corresponded to C=C stretching vibration of the quinoid and benzenoid rings in PANI.[19,20] The peaks at 1298, 1242, and 1134 cm^{-1} were assigned to the C–N stretching vibration, the $C–N^{+\bullet}$ stretching vibration in the polaron form of PANI emeraldine salt, and the C=N stretching vibration, respectively.[20,21] The peaks at 1057, 949, 872, and 773 cm^{-1} were assigned to P–O bonds, Mo=O terminal bonds, vertex Mo–O–Mo bonds, and edge Mo–O–Mo bonds in POM clusters, respectively.[4]

Fig. 4a shows the CV curves of POM-PANI/nanopillar, PANI/nanopillar, and POM-PANI/flat (with flat structured polymeric films) electrodes in 0.5 M H_2SO_4. The POM-PANI/nanopillar electrode exhibited multiple reversible redox peaks, whereas the PANI/nanopillar electrode did not, which is indicative of successful entrapment of POMs into the PANI matrix. The current of the POM-PANI/nanopillar electrode is much higher than that of the POM-PANI/flat electrode due to the effect of the 1D nanostructure. Peak-to-peak potential separation of the POM-PANI/nanopillar electrode calculated using redox peaks, was 15 mV. This finding indicates that the POM-PANI/nanopillar electrode is capable of delivering a rapid electron transfer rate in a manner close to the kinetic ideal for a two-electron electrochemical reaction.[22] In addition, Tafel analysis was performed on the POM-PANI/nanopillar electrode to investigate its kinetic behavior. As shown in the inset of Fig. 4a, Tafel plots were obtained using the reduced form of the Butler–Volmer equation as follows:[23]

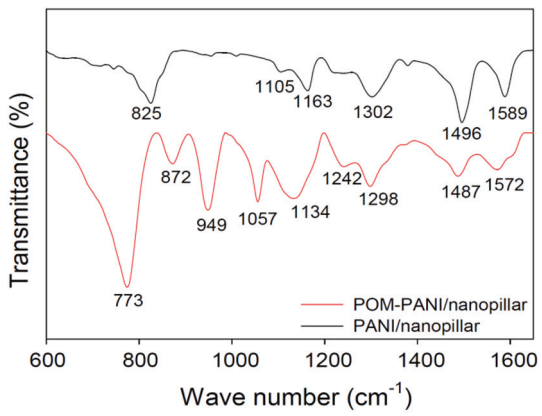

Fig. 3 FTIR spectra of POM-PANI/nanopillar and PANI/nanopillar films.

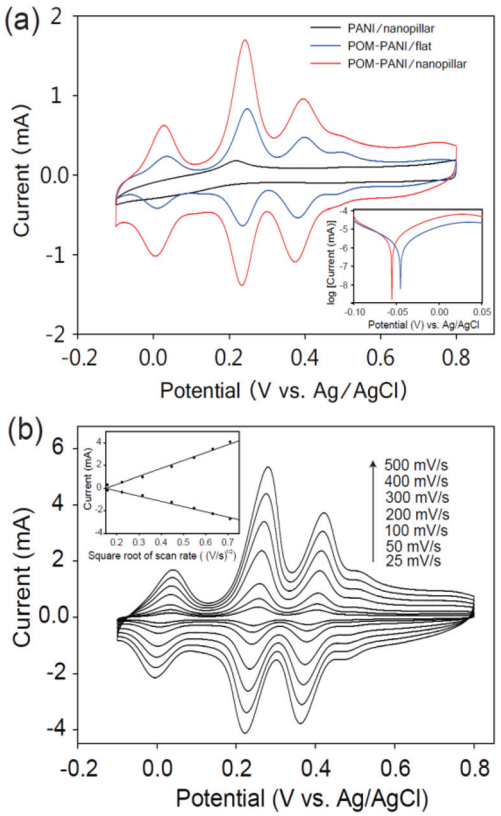

Fig. 4 (a) CV curves of PANI/nanopillar, POM-PANI/flat, POM-PANI/nanopillar electrodes in solution containing 0.5 M H_2SO_4 at a scan rate of 50 mV s^{-1}. Inset: Tafel plots of POM-PANI/flat and POM-PANI/nanopillar electrodes obtained from CV curves. (b) CVs of a POM-PANI/nanopillar electrode in solution containing 0.5 M H_2SO_4 at different scan rates (25, 50, 100, 200, 300, 400, and 500 mV s^{-1}). Inset: plot of I_p *versus* square root of scan rates at a POM-PANI/nanopillar electrode.

$$\log i = \log i_o + \frac{\alpha_A nF}{2.303RT}\eta \quad (1)$$

where η is the overpotential, i is the exchange current density, α_A is the symmetry factor, and other symbols have convention-

al meanings. Obviously, the introduction of a nanopillar array reduced onset potential from −45 mV of POM-PANI/flat to −55 mV of POM-PANI/nanopillar. This indicates that the nanopillar structure on POM-PANI/nanopillar enabled more efficient and faster charge transfer than POM-PANI/flat.

The CV curves of the POM-PANI/nanopillar electrode were also investigated at different scan rates (25 to 500 mV s^{-1}; Fig. 4b). As scan rates increased, the current response increased with well-defined three pairs of redox peaks. A linear dependence was obtained for the relationships between anodic or cathodic peak currents and the square root of the scan rate (R^2 = 0.9986 and 0.9995 for anodic and cathodic peaks, respectively). Consequently, redox reactions were attributed to semi-infinite linear diffusion at the surface of the POM-PANI/nanopillar electrode.[23]

Fig. 5 presents the chronoamperograms of the oxidation reactions of POMs on a representative POM-PANI/nanopillar and POM-PANI/flat. Current–time responses were measured under Cottrell conditions according to the following equation:[23]

$$I = \frac{FAD^{1/2}C}{\pi^{1/2}t^{1/2}} \quad (2)$$

where I is the current, F is the Faraday's constant, D is the diffusion coefficient, C is the bulk concentration of H_2SO_4, A is the electrode area, and t is time. As the electro-oxidation occurs on the electrode surface, the current plot is inversely proportional to $t^{1/2}$. The diffusion coefficient was calculated from the linear slope of I *versus* $t^{-1/2}$ curves, as shown in Fig. 5b. POM-PANI/nanopillar had a diffusion coefficient of 2.8 × 10^{-12} cm^2 s^{-1}, which was higher than that of POM-PANI/flat (8.6 × 10^{-13} cm^2 s^{-1}). This result implies that the nanopillar structure facilitated the diffusion of electrolyte and thus, enhanced the redox reaction.

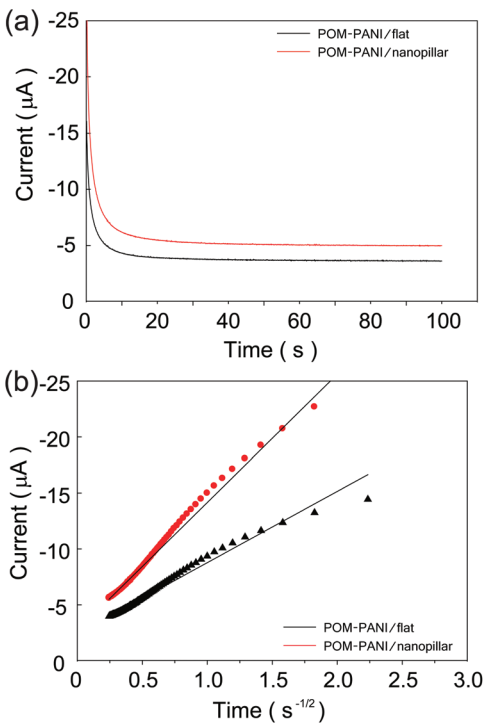

Fig. 5 (a) Chronoamperograms of POM-PANI/flat and POM-PANI/nanopillar electrodes and (b) calibration curves of the current *versus* $t^{-1/2}$ for POM-PANI/flat and POM-PANI/nanopillar electrodes.

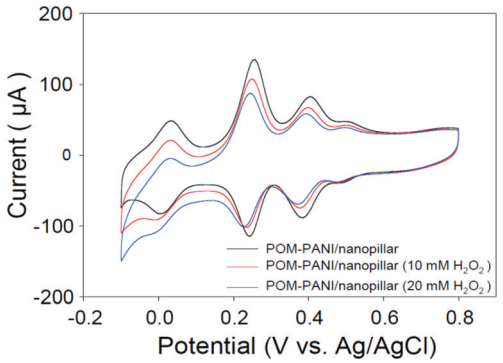

Fig. 6 CVs of a POM-PANI/nanopillar electrode in the absence and presence of H_2O_2 (10 mM and 20 mM) at a scan rate of 50 mV s^{-1}.

In order to evaluate electrocatalytic performance, the POM-PANI/nanopillar electrode was incorporated into a flow injection biosensor device and the electrocatalytic reduction of H_2O_2 was measured by flow-injection amperometry. The electrocatalytic reduction of H_2O_2 by the POM-PANI/nanopillar electrode was initially investigated using CV measurements (Fig. 6). The POM-PANI/nanopillar electrode showed good electrocatalytic activity for the reduction of hydrogen peroxide at concentrations from 10 to 20 mM. The electrocatalytic reaction was observed at the reduction peak of the redox pair of POM. Fig. 7a shows a typical amperometric response of the POM-PANI/nanopillar electrode to the successive flow injection of H_2O_2 at an operating potential of 0.02 V. As shown in Fig. 7b, the current responses of the POM-PANI/nanopillar electrode were plotted with respect to the H_2O_2 concentration in the range of 0.1 to 20 mM. The POM-PANI/nanopillar biosensor exhibited wide-range linear characteristics with high sensitivity (6.3 μA mM^{-1} cm^{-2}). The sensitivity of the POM-PANI/nanopillar biosensor was greater than that of the POM-PANI/nanopillar biosensor (2.0 μA mM^{-1} cm^{-2}) and was also higher than those of other enzymeless biosensors, including Co_3O_4 cube,[14] $H_4Fe_4(PMo_9O_{34})_2^{6-}$-doped conducting polymer,[24] $PFeW_{11}O_{39}^{4-}$-doped silica gel.[25] All responses reached the peak current within ~3 s, indicating a rapid response due to enhanced charge transfer. In addition, the limit of detection (LOD) was calculated at a signal-to-noise ratio of 3 : 8.1 μM for the POM-PANI/nanopillar electrode. This result indicates that the POM-PANI/nanopillar biosensor shows substantial potential as an electrochemical biosensor due to its high sensitivity, low LOD, and rapid response time.

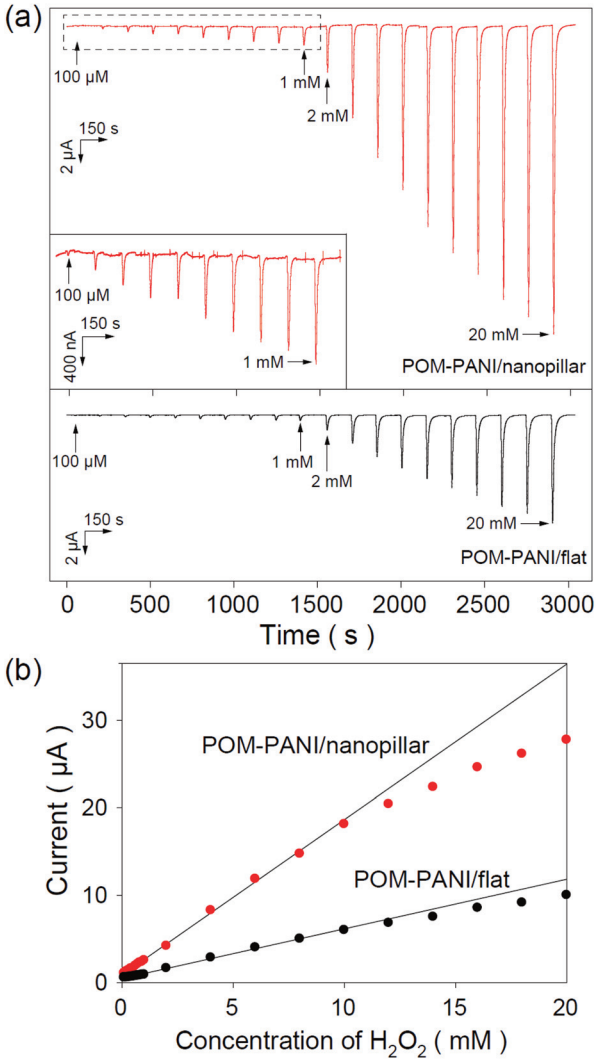

Fig. 7 (a) Amperometric responses of POM-PANI/nanopillar and POM-PANI/flat electrode-based fluidic biosensor devices with increasing concentration of H_2O_2 ranging from 0.1 to 20 mM in the flow injection system at 0.02 V. (b) Calibration curves of the electrocatalytic current on the concentration of H_2O_2 at POM-PANI/nanopillar and POM-PANI/flat electrode-based fluidic biosensor devices.

4. Conclusions

We prepared highly ordered POM-doped PANI nanopillar arrays and characterized their non-enzymatic electrochemical properties for the detection of H_2O_2 in microfluidic systems. The employment of co-electrodeposition enabled the entrapment of POMs into the PANI matrix and fully coated the surfaces of 1D Au-coated polymer substrates. The devised POM-PANI/nanopillar electrode was incorporated into microfluidic channels and showed excellent electrocatalytic activity for the reduction of hydrogen peroxide with high sensitivity, low detection limit, rapid response time, and robust electrocatalytic activity. This sensor performance was attributed to the large surface area of the 1D nanostructure to the multiple redox reactions of POMs, and to the rapid and efficient ion and electron transfer during the electrochemical process.

Acknowledgements

This work was supported by the National Research Foundation of Korea (NRF) Grant funded by the Korean Government (MSIP) (No. 2014R1A5A2010008 and No. 2015R1C1A1A02036556) and the BioNano Health-Guard Research Center funded by the Ministry of Science, ICT & Future Planning (MSIP) of Korea as the Global Frontier Project (Grant number H-GUARD_2013M3A6B2078945). This research was also supported by the Ministry of Trade, Industry & Energy (MOTIE), Korea Institute for Advancement of Technology (KIAT) through the Encouragement Program for The Industries of Economic Cooperation Region.

Notes and references

1 X. López, J. J. Carbó, C. Bo and J. M. Poblet, *Chem. Soc. Rev.*, 2012, **41**, 7537–7571.
2 H. N. Miras, J. Yan, D.-L. Long and L. Cronin, *Chem. Soc. Rev.*, 2012, **41**, 7403–7430.
3 Y.-F. Song and R. Tsunashima, *Chem. Soc. Rev.*, 2012, **41**, 7384–7402.
4 M. Yang, B. G. Choi, S. C. Jung, Y.-K. Han, Y. S. Huh and S. B. Lee, *Adv. Funct. Mater.*, 2014, **24**, 7301–7309.
5 X.-B. Han, Y.-G. Li, Z.-M. Zhang, H.-Q. Tan, Y. Lu and E.-B. Wang, *J. Am. Chem. Soc.*, 2015, **137**, 5486–5493.
6 N. Anwar, M. Vagin, F. Laffir, G. Armstrong, C. Dickinson and T. McCormac, *Analyst*, 2012, **137**, 624–630.
7 W. Zhang, D. Du, D. Gunaratne, R. Colby, Y. Lin and J. Laskin, *Electroanalysis*, 2014, **26**, 178–183.
8 Y.-Y. Ling, Q.-A. Huang, M.-S. Zhu, D.-X. Feng, X.-Z. Li and Y. Wei, *J. Electroanal. Chem.*, 2013, **693**, 9–15.
9 B. Wang, R.-Q. Meng, L.-X. Xu, L.-X. Wu and L.-H. Bi, *Anal. Methods*, 2013, **5**, 885–890.
10 Y. Xiang, S. Lu and S. P. Jiang, *Chem. Soc. Rev.*, 2012, **41**, 7291–7321.
11 A. Nisar, J. Zhuang and X. Wang, *Chem. Mater.*, 2009, **21**, 3745–3751.
12 X.-L. Wang, Y.-L. Wang, W.-K. Miao, M.-B. Hu, J. Tang, W. Yu, Z.-Y. Hou, P. Zheng and W. Wang, *Langmuir*, 2013, **29**, 6537–6545.
13 G. M. Suppes, B. A. Deore and M. S. Freund, *Langmuir*, 2008, **24**, 1064–1069.
14 S. Xia, M. Yu, J. Hu, J. Feng, J. Chen, M. Shi and X. Weng, *Electrochem. Commun.*, 2014, **40**, 67–70.
15 F. Xi, D. Zhao, X. Wang and P. Chen, *Electrochem. Commun.*, 2013, **26**, 81–84.
16 R. Liu, S. Li, X. Yu, G. Zhang, S. Zhang, J. Yao, B. Keita, L. Nadjo and L. Zhi, *Small*, 2012, **8**, 1398–1406.
17 B. Haghighi, H. Hamidi and L. Gorton, *Electrochim. Acta*, 2010, **55**, 4750–4757.

18 K. G. Lee, B. G. Choi, B. I. Kim, T. Shyu, M. S. Oh, S. G. Im, S.-J. Chang, T. J. Lee, N. A. Kotov and S. J. Lee, *Adv. Mater.*, 2014, **26**, 6119–6124.
19 J. Fei, Y. Cui, X. Yan, Y. Yang, K. Wang and J. Li, *ACS Nano*, 2009, **3**, 3714–3718.
20 M. Li, X. Huang, C. Wu, H. Xu, P. Jiang and T. Tanaka, *J. Mater. Chem.*, 2012, **22**, 23477–23484.
21 C. Vaghela, M. Kulkarni, M. Karve, R. Aiyer and S. Haram, *RSC Adv.*, 2014, **4**, 59716–59725.
22 M. Sadakane and E. Steckhan, *Chem. Rev.*, 1998, **98**, 219–238.
23 A. J. Bard and L. R. Faulkner, *Electrochemical Methods: Fundamentals and Applications*, Wiley, New York, 2001.
24 G. L. Turdean, A. Curulli, I. C. Popescu, C. Rosu and G. Palleschi, *Electroanalysis*, 2002, **14**, 1550–1556.
25 H. Hamidi, E. Shams, B. Yadollahi and F. K. Esfahani, *Electrochim. Acta*, 2009, **54**, 3495–3500.